Journal of Materials Chemistry A

Accepted Manuscript

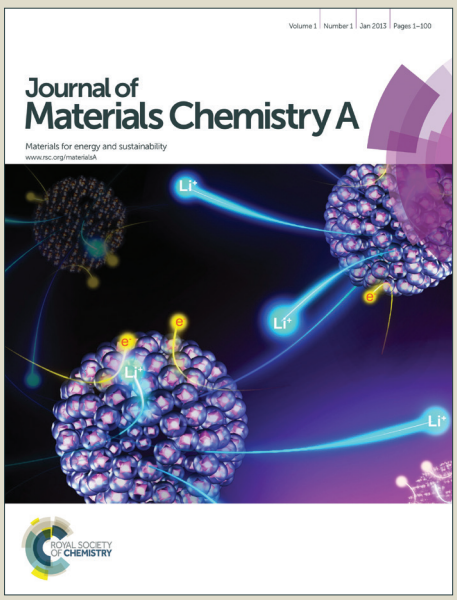

ROYAL SOCIETY OF CHEMISTRY

www.rsc.org/materialsA

Journal Name

RSCPublishing

COMMUNICATION

High-Performance Hole-Transporting Layer-Free Conventional Perovskite/Fullerene Heterojunction Thin-Film Solar Cells

Cite this: DOI: 10.1039/xoxxoooooox

Received ooth January 2012,
Accepted ooth January 2012

www.rsc.org/

Kai-Wei Tsai,[a,c] Chu-Chen Chueh,[a] Spencer T. Williams,[a] Ten-Chin Wen,[c] and Alex K.Y. Jen*[a]

A high-performance hole-transporting layer (HTL)-free conventional perovskite/fullerene heterojunction thin-film PVSC was demonstrated. We revealed that perovskite can modify the work function of ITO, leading to sufficient charge extraction efficiency at the ITO/perovskite interface. Combined with the high conductivity of ITO, a PCE of > 11% with a high open-circuit voltage (*Voc*) of 1.01 V was achieved.

The rapid development of organometal halide perovskite ($CH_3NH_3PbI_3$) solar cells (PVSCs) has attracted worldwide attention due to the material's high absorption coefficient, small exciton binding energy, and long carrier diffusion length. Quickly increasing power conversion efficiencies (PCE), from 3.81% to 19.3%, have been realized in just a few years.[1-6] Because of their solution processability and simple device fabrication compared to purely inorganic photovoltaics, hybrid organic-inorganic perovskites have been envisioned as high-potential materials for commercial solar energy production.[7]

At present, PVSCs are mainly fabricated in two kinds of device architectures: mesoporous and thin-film. These can be further defined as conventional (p-i-n) or inverted (n-i-p) types based on the sequence of charge-transporting interlayers (CTLs). For inverted PVSCs, the most frequently used electron-transporting layers (ETLs) are based on transition metal oxides (TiO_2 and ZnO) while hole-transporting layers (HTLs) are mainly based on organic semiconductors such as (2,2′,7,7′-tetrakis(N,N-di-p-methoxyphenylamine)-9,9′-spirobi-fluorene (spiro-OMeTAD).[8-10] An impressive PCE of 19.3% has been realized in a planar, inverted PVSC with the use of yttrium doped compact TiO_2 and spiro-OMeTAD *via* interfacial engineering.[6]

More recent studies have revealed that the HTL can be exempted from inverted PVSCs due to the decent hole conductivity of $CH_3NH_3PbI_3$ ($MAPbI_3$).[11-14] Such HTL-free PVSCs are able to achieve PCEs over 10% by optimizing perovskite crystallization and device engineering.[14-17] For these high-performance inverted HTL-free PVSCs, carbon and gold (Au) are the commonly used anodes since their work functions (WFs, ~5.0-5.2 eV) match reasonably well with the valence band (VB, ~5.4 eV) of $CH_3NH_3PbI_3$, establishing energetic alignment for efficient hole extraction. This also minimizes potential loss across the perovskite/anode interface, especially without HTL.

Compared to inverted PVSCs, conventional devices can be fabricated through a relatively low-temperature process (~ 100 °C) because of the employment of organic-based CTLs, such as PEDOT:PSS HTL and $PC_{61}BM$ ETL.[18-23] Unlike inverted PVSCs, in which the HTL can be exempted because the hole extraction barrier ($\Delta\Phi_h$) can be alleviated with high WF carbon or Au anodes, HTLs with deep-lying energy levels seem to be required for conventional PVSCs due to the high $\Delta\Phi_h$ at the ITO/perovskite interface (**Fig 1**). The poorly aligned energy levels will cause great potential loss and reduction of hole extraction efficiency in resulting devices.

In this study, we describe a high-performance HTL-free conventional perovskite/fullerene heterojunction thin-film PVSC with a PCE_{MAX} of 11.02% and a high open-circuit voltage (*Voc*) of 1.01 V (**Fig. 1**). We adopted the solvent-washing technique reported by Seok *et al.* for the deposition of $MAPbI_3$, which enables uniform morphology with nearly full surface coverage.[5] We showed that ITO substrates can quench perovskite's photoluminescence to a degree comparable to that from PEDOT:PSS HTL, which suggests that the ITO interface can extract charge from $MAPbI_3$ efficiently. The results from X-ray photoelectron spectroscopy (XPS) suggest that the MA^+ cation can form hydrogen bonding with the ITO surface resulting in a slight increased WF (0.3 eV). All these results signify that the ITO/perovskite interface can afford high-performance HTL-free conventional PVSCs in spite of mismatched energy levels. It is interesting to note that, during the preparation of this manuscript, Kelly *et al.* reported a high-performance (13.5%) ETL-free inverted perovskite/HTL heterojunction thin-film PVSC, [24] in which a large *Voc* of ~ 1 V could be observed notwithstanding the reversed device polarity

as compared to our devices. Sequential deposition was employed to grow perovskite in this case, and unreacted PbI_2 might remain at the ITO/perovskite interface.[25] In addition to the distinct chemical interaction at the interface, Chen *et al.* have demonstrated that PbI_2 plays a unique role electronically leading to an interface different from the one studied here. However, based on our and Kelly's findings, it can be concluded that the ITO/perovskite interface possesses superior charge dissociation/extraction efficiency and barrier-less like contact despite mismatched energy levels, probably partly arising from ITO's high conductivity (1.3×10^4 S/cm).[26]

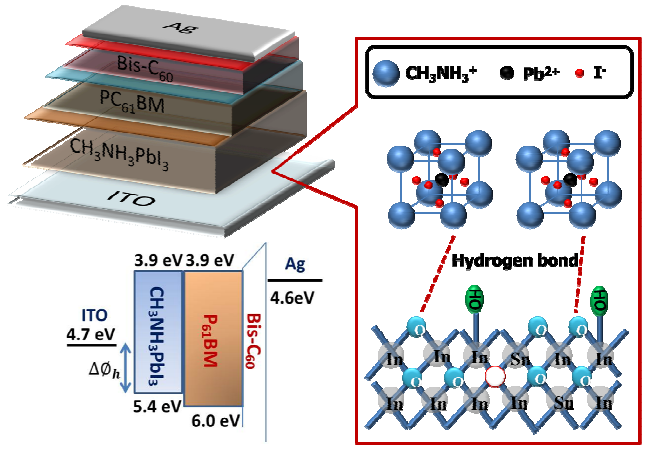

Fig. 1 The device configuration, energy diagram, and illustration of perovskite/ITO interface of conventional HTL-Free PVSC.

To realize the feasibility of conventional HTL-free PVSCs, we fabricated perovskite/fullerene heterojunction thin-film devices with the configuration of ITO/$MAPbI_3$/$PC_{61}BM$/Bis-C_{60}/Ag (**Fig. 1**).[4, 22, 27] The *J-V* curve of the top-performing PVSC is shown in **Fig. 2 (a)** and average device performance is summarized in **Table S1** (supporting information). Impressively, the conventional HTL-free PVSC shows a PCE_{MAX} of 11.02% with a *Voc* of 1.01 V, a short-circuit current (*Jsc*) of 15.69 mA/cm^2, and a fill factor (FF) of 0.70. The high *Voc* of the device is beyond our initial expectation because of the large energy barrier ($\Delta\Phi_h$) at the ITO/perovskite interface due to mismatched energy levels, as can be seen in the device energy diagram in **Fig. 1**. In principle, this may create an Schottky barrier at the interface and thus potential loss, which would reduce *Voc*. However, the large *Voc* (1.01 V) obtained herein suggests a barrier-less like contact at the ITO/perovskite interface, which may result from ITO WF modification.

Compared to devices using a PEDOT:PSS HTL (**Fig. S1**),[28] the conventional HTL-free PVSC has lower *Jsc* and FF. This may result from increased contact resistance and poor charge selectivity at the ITO/perovskite interface due to ITO's high-lying WF (located in the middle of perovskite's band-gap) and the high conductivity of ITO, respectively. In this regard, interfacial recombination loss restrains device performance.

Shown in **Fig. 2 (b)** is the external quantum efficiency (EQE) of the top-performing HTL-free PVSC. The integrated *Jsc* (15.24 mA/cm^2) from the EQE spectra is in good agreement with *Jsc* (15.69 mA/cm^2). The broad, intense photo-response from 330 nm to 780 nm is consistent with the panchromatic absorption of $MAPbI_3$. Even without an HTL, ~70% EQE values were achieved, suggesting efficient hole extraction.

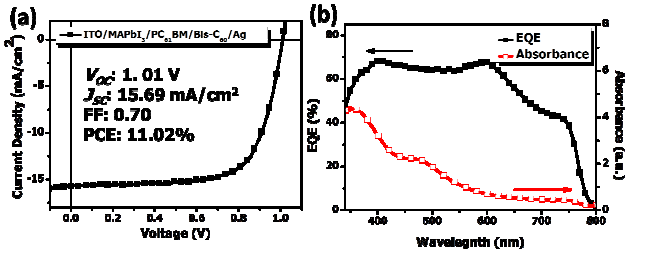

Fig. 2 (a) *J-V* curve and (b) EQE of the studied HTL-free PVSC along with the UV-Vis spectra of perovskite.

Crystallization of perovskite on ITO was examined by X-ray diffraction (XRD) and the characteristic patterns are presented in **Fig. 3(a)**. For comparison, $MAPbI_3$ thin-films on glass and PEDOT:PSS HTL deposited through same procedure were also prepared. As is clearly shown, all samples have prominent diffraction peaks at 14.15° and 28.46° 2θ, corresponding to the (110) and (220) planes of $MAPbI_3$. Peaks at 30.15° and 35.23° 2θ in the ITO/$MAPbI_3$ and ITO/PEDOT:PSS/$MAPbI_3$ samples represent the (222) and (004) lattice planes of ITO. Comparable intensity of characteristic $MAPbI_3$ reflections in ITO/$MAPbI_3$ and ITO/PEDOT:PSS/$MAPbI_3$ samples manifests that $MAPbI_3$ can form a highly crystalline film directly on an ITO substrate.

It has been acknowledged that perovskite surface coverage is heavily dependent upon crystallization kinetics.[29] The scanning electron microscopy (SEM) image shows high surface coverage on bare ITO **(Fig. 3(b))**. Moreover, perovskite crystal domain size, surface morphology, and coverage on ITO is similar to the perovskite film deposited on PEDOT:PSS/ITO (**Fig. S2**). This implies that the surface energy of ITO allows the uniform growth of crystalline perovskite. That said, this excellent film quality is also partly due to the homogenous nucleation encouraged by the *in-situ* addition of non-polar solvent during spin-coating, which is the step that distinguishes the solvent-washing technique from other prevailing perovskite deposition methods.[5] This may diminish the influence of surface energy on perovskite crystallization. The high surface coverage and homogeneous morphology of the $MAPbI_3$ film on ITO and ITO/PEDOT:PSS substrates prevent direct contact between ITO and $PC_{61}BM$, avoiding shorting.[30]

Fig. 3(c) displays PL spectra of glass/$MAPbI_3$, ITO/$MAPbI_3$, and ITO/PEDOT:PSS/$MAPbI_3$. For glass/$MAPbI_3$, a strong perovskite emission signal at 770 nm was observed. When the glass substrate was replaced by ITO coated glass, this was greatly reduced. This quenching is comparable to ITO/PEDOT:PSS/$MAPbI_3$. Combined with the high PCE of the HTL-free perovskite/fullerene heterojunction thin-film device, efficient hole extraction at the ITO/$MAPbI_3$ interface can be inferred.

As mentioned, the conventional HTL-free PVSC possessed a high *Voc* (1.01 eV) despite a high $\Delta\Phi_h$ at the ITO/perovskite interface. This may imply that interaction occurs between the deposited perovskite and ITO to modify this barrier. To explore this phenomenon, XPS was conducted as is shown in **Fig. 4**.

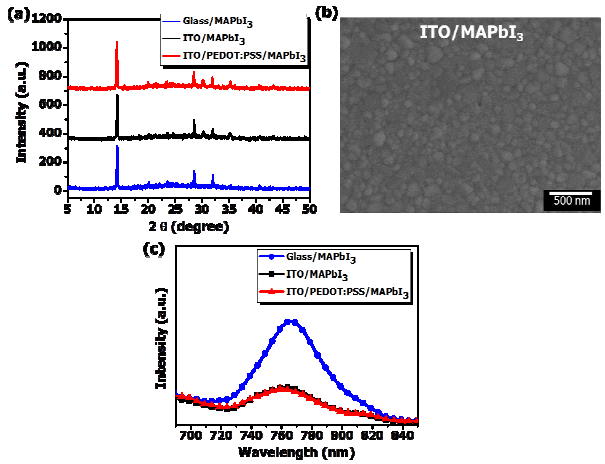

Fig. 3 (a) XRD patterns & (c) PL spectra: glass/$MAPbI_3$, ITO/$MAPbI_3$, & ITO/PEDOT:PSS/$MAPbI_3$. (b) SEM image of ITO/$MAPbI_3$.

Thin perovskite and MAI films were prepared by diluting the precursor solution (0.05 M, 0.08 M, and 0.1 M $MAPbI_3$; 0.05 M MAI). The thickness of the 0.1 M perovskite thin film was ~2.8 nm as measured by atomic force microscopy. WF measurement was performed in the secondary electron cut-off region (**Fig. 4(a)**). Cut-offs of ITO/$MAPbI_3$ (0.05 M) and ITO/MAI shifted toward a lower binding energy compared to bare ITO, representing a change of ITO's WF (4.7 to 5.0 eV).

Shown in **Fig. 4(b)** are O 1s core level spectra of ITO, ITO/$MAPbI_3$ (0.1 M), ITO/$MAPbI_3$ (0.08 M), ITO/$MAPbI_3$ (0.05 M), and ITO/MAI. Compared to the bare ITO substrate, the contribution from the high binding energy shoulder of the O 1s peak at ~532 eV increased slightly in all modified systems accompanied by a slight overall shift to higher binding energy which is, to a first approximation, what we would expect from both surface protonation (OH formation) and hydrogen bonding.[31, 32] That said, in ITO both the exact physical source of each component of the O 1s manifold and the nature of the contribution from OH remain a matter of general contention in the field.[33] With that in mind, we present a deconvolution of the O 1s spectra in Fig. S3 *via* similar constraints used by Kim *et al.*,[33] but based on the O 1s manifold alone we only correlate perovskite and MAI deposition with the general increase in cationic character typically associated with surface protonation and hydrogen bonding.[32]

As presented in **Fig. 4(c)**, there was a shift in the N 1s signal toward lower binding energy in samples made with adequately dilute perovskite precursor solutions (0.08 M and 0.05 M). This shift to lower binding energy as the precursor solution is diluted is opposite to the shift we would expect from the increase in cationic character hydrogen bonding is typically assumed to engender,[32] but this is unsurprising in this system because the entire population of nitrogen containing molecules (MA^+) are already cationic Lewis acids. Electron density surrounding nitrogens participating in hydrogen bonds with the ITO surface may increase relative to the dynamic hydrogen bonding environment MA^+ exists in within the $MAPbI_3$ lattice.[33] The difference between these two bonding environments is complex as hydrogen bond number and angle change in each system, and nitrogen's electronegativity lies between that of iodide and oxygen making bond polarity variable as well.[33] That said, the correlation between this shift, the change in ITO's WF, and the changes in the O 1s manifold implicate methyl ammonium as key in possible interaction between perovskite and ITO. It has been found that simple protonation of the ITO surface can increase work function,[34, 35] but it would be surprising if this shifted N 1s signal originated solely from the highly volatile fully deprotonated MA^+, suggesting that hydrogen bonding is a more plausible mechanism of interaction.

While we attempted to fabricate thinner films to confirm this trend from solutions with lower concentrations, challenges controlling the $MAPbI_3$ phase transformation prevented reliable deposition with solutions below 0.05 M. To more selectively observe possible MA^+-ITO interaction, we removed lead iodide from the already dilute precursor solution. This produced the same shift in ITO's WF observed in the case of perovskite. The N 1s signal in the MAI/ITO film shifted to an even lower binding energy than any of the $MAPbI_3$/ITO films. Although there is undoubtedly a contribution from the change in bonding within the MAI phase itself, we ascribe the small secondary peak appearing within the N 1s manifold at low binding energy to interaction between MA^+ and the ITO surface.

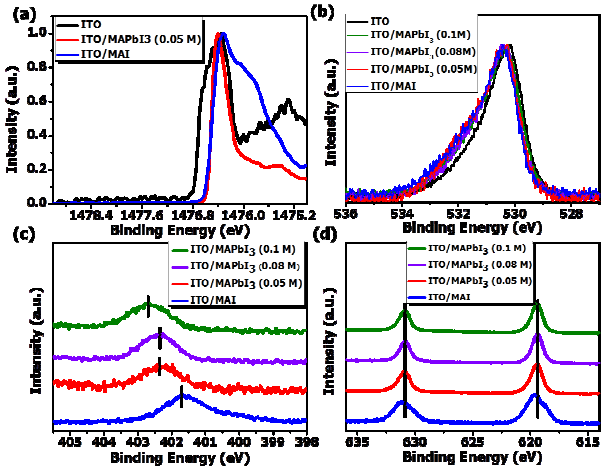

Fig. 4 XPS spectra of (a) Secondary electron cut-off: ITO, ITO/$MAPbI_3$ (0.05 M), & ITO/MAI (b) O 1s spectra: ITO, ITO/$MAPbI_3$ (0.1 M), ITO/$MAPbI_3$ (0.08 M), ITO/$MAPbI_3$ (0.05 M), & ITO/MAI (c) N 1s and (d) I $3d_{5/2}$ & $3d_{3/2}$ core level signals: ITO/$MAPbI_3$ (0.1 M), ITO/$MAPbI_3$ (0.08 M), ITO/$MAPbI_3$ (0.05 M), & ITO/MAI.

The negligible change in chemical shift of I $3d_{5/2}$ and $3d_{3/2}$ core levels among the ITO/$MAPbI_3$ samples in **Fig. 4(d)** manifests that the observed shifts do not result from charging or

band bending.[36] The slight difference of binding energy and shape between I $3d_{5/2}$ and $3d_{3/2}$ signals in ITO/MAI and ITO/$MAPbI_3$ samples likely results from the change in iodide's bonding environment, but the shift in the N 1s signal is greater than the small change in iodide's peak position. We posit that together these data point to WF modification through the generation of an interfacial dipole stabilized by hydrogen bonding between MA^+ and ITO, but we do not as of yet completely exclude simple protonation[37] or other mechanisms of chemisorption because of the complexity inherent to the system and the challenges inherent in sample preparation from solution.

The high-performance (13.5%) and large *Voc* (~1 V) of the inverted ETL-free PVSC reported by Kelly *et al.*[24] combined with our findings demonstrate that the ITO/perovskite interface possesses superior charge dissociation/extraction efficiency. These results also reveal the barrier-less like contact between ITO and perovskite despite mismatched energy levels. With regard to the non-excitonic nature of perovskite, the high electrical conductivity of ITO might be a key contributor to the interface's efficacy. This understanding is important for the future development of high-performance HTL/ETL-free PVSCs.

Conclusions

In this communication, we have demonstrated a high-performance HTL-free conventional perovskite/fullerene heterojunction thin-film PVSC with PCE_{MAX} of 11.02%. It was revealed that the ITO substrate can quench perovskite photoluminescence (PL) as well as a PEDOT:PSS HTL, suggesting its sufficient charge extraction efficiency from the $MAPbI_3$ thin-film. More interestingly, despite the mismatched energy levels at the ITO/perovskite interface, the device can still afford a high *Voc* of 1.01 V. It was found from XPS that the MA^+ cation of $MAPbI_3$ perovskite can interact with unprotonated oxygen at the ITO surface, resulting in hydrogen bonding and a slightly increased ITO WF (0.3 eV). Such WF tuning combined with the high conductivity of ITO result in the observed high *Voc*. The successful demonstration of high-performance conventional HTL-free PVSCs in this study both enables simplified device architectures and underscores the important role perovskite interfaces play in PVSCs.

Notes and references

[a]*Department of Materials Science and Engineering, University of Washington, Seattle, WA 98195-2120, USA.*
[b]*Department of Chemical Engineering, National Cheng Kung University, Tainan, 70101, Taiwan.*

This work is supported by the Office of Naval Research (N00014-14-1-0170), the Department of Energy Sun Shot (DE-EE0006710), and the Asian Office of Aerospace R&D (FA2386-11-1-4072). A. K.-Y. Jen thanks the Boeing-Johnson Foundation for financial support. K.W.T thanks the financial support from the Ministry of Science and Technology (103-2917-I-006-087-). S.T.W. thanks the support from the National Science Foundation (DGE-0718124 and DGE-1256082).

1. A. Kojima, K. Teshima, Y. Shirai and T. Miyasaka, *J. Am. Chem. Soc.*, 2009, **131**, 6050-6051.
2. S. D. Stranks, G. E. Eperon, G. Grancini, C. Menelaou, M. J. P. Alcocer, T. Leijtens, L. M. Herz, A. Petrozza and H. J. Snaith, *Science*, 2013, **342**, 341-344.
3. G. Xing, N. Mathews, S. Sun, S. S. Lim, Y. M. Lam, M. Grätzel, S. Mhaisalkar and T. C. Sum, *Science*, 2013, **342**, 344-347.
4. P.-W. Liang, C.-Y. Liao, C.-C. Chueh, F. Zuo, S. T. Williams, X.-K. Xin, J. Lin and A. K. Y. Jen, *Adv. Mater.*, 2014, **26**, 3748-3754.
5. N. J. Jeon, J. H. Noh, Y. C. Kim, W. S. Yang, S. Ryu and S. I. Seok, *Nat Mater*, 2014, **13**, 897-903.
6. H. Zhou, Q. Chen, G. Li, S. Luo, T.-b. Song, H.-S. Duan, Z. Hong, J. You, Y. Liu and Y. Yang, *Science*, 2014, **345**, 542-546.
7. J. H. Kim, S. T. Williams, N. Cho, C.-C. Chueh and A. K. Y. Jen, *Adv. Eenergy Mater.*, 2014, DOI: 10.1002/aenm.201401229, n/a-n/a.
8. J. Burschka, N. Pellet, S.-J. Moon, R. Humphry-Baker, P. Gao, M. K. Nazeeruddin and M. Gratzel, *Nature*, 2013, **499**, 316-319.
9. M. M. Lee, J. Teuscher, T. Miyasaka, T. N. Murakami and H. J. Snaith, *Science*, 2012, **338**, 643-647.
10. D. Liu and T. L. Kelly, *Nat Photon*, 2014, **8**, 133-138.
11. L. Etgar, P. Gao, Z. Xue, Q. Peng, A. K. Chandiran, B. Liu, M. K. Nazeeruddin and M. Grätzel, *J. Am. Chem. Soc.*, 2012, **134**, 17396-17399.
12. W. A. Laban and L. Etgar, *Energ. Environ. Sci.*, 2013, **6**, 3249-3253.
13. Z. Li, S. A. Kulkarni, P. P. Boix, E. Shi, A. Cao, K. Fu, S. K. Batabyal, J. Zhang, Q. Xiong, L. H. Wong, N. Mathews and S. G. Mhaisalkar, *ACS Nano*, 2014, **8**, 6797-6804.
14. A. Mei, X. Li, L. Liu, Z. Ku, T. Liu, Y. Rong, M. Xu, M. Hu, J. Chen, Y. Yang, M. Grätzel and H. Han, *Science*, 2014, **345**, 295-298.
15. S. Aharon, S. Gamliel, B. E. Cohen and L. Etgar, *PCCP*, 2014, **16**, 10512-10518.
16. F. Hao, C. C. Stoumpos, Z. Liu, R. P. H. Chang and M. G. Kanatzidis, *J. Am. Chem. Soc.*, 2014, **136**, 16411-16419.
17. J. Shi, Y. Luo, H. Wei, J. Luo, J. Dong, S. Lv, J. Xiao, Y. Xu, L. Zhu, X. Xu, H. Wu, D. Li and Q. Meng, *ACS Appl. Mater. Inter.*, 2014, **6**, 9711-9718.
18. J.-Y. Jeng, Y.-F. Chiang, M.-H. Lee, S.-R. Peng, T.-F. Guo, P. Chen and T.-C. Wen, *Adv. Mater.*, 2013, **25**, 3727-3732.
19. O. Malinkiewicz, A. Yella, Y. H. Lee, G. M. Espallargas, M. Graetzel, M. K. Nazeeruddin and H. J. Bolink, *Nat Photon*, 2014, **8**, 128-132.
20. Z. Xiao, Q. Dong, C. Bi, Y. Shao, Y. Yuan and J. Huang, *Adv. Mater.*, 2014, **26**, 6503-6509.
21. J. You, Z. Hong, Y. Yang, Q. Chen, M. Cai, T.-B. Song, C.-C. Chen, S. Lu, Y. Liu, H. Zhou and Y. Yang, *ACS Nano*, 2014, **8**, 1674-1680.
22. C.-C. Chueh, C.-Y. Liao, F. Zuo, S. T. Williams, P.-W. Liang and A. K. Y. Jen, *J. Mater. Chem. A*, 2015, DOI: 10.1039/C4TA05012F.
23. Z. Xiao, C. Bi, Y. Shao, Q. Dong, Q. Wang, Y. Yuan, C. Wang, Y. Gao and J. Huang, *Energ. Environ. Sci.*, 2014, **7**, 2619-2623.
24. D. Liu, J. Yang and T. L. Kelly, *J. Am. Chem. Soc.*, 2014, **136**, 17116-17122.
25. Q. Chen, H. Zhou, T.-B. Song, S. Luo, Z. Hong, H.-S. Duan, L. Dou, Y. Liu and Y. Yang, *Nano Lett.*, 2014, **14**, 4158-4163.
26. H. Hosono, H. Ohta, M. Orita, K. Ueda and M. Hirano, *Vacuum*, 2002, **66**, 419-425.
27. F. Zuo, S. T. Williams, P.-W. Liang, C.-C. Chueh, C.-Y. Liao and A. K. Y. Jen, *Adv. Mater.*, 2014, **26**, 6454-6460.
28. J. Seo, S. Park, Y. Chan Kim, N. J. Jeon, J. H. Noh, S. C. Yoon and S. I. Seok, *Energ. Environ. Sci.*, 2014, **7**, 2642-2646.
29. S. T. Williams, F. Zuo, C.-C. Chueh, C.-Y. Liao, P.-W. Liang and A. K. Y. Jen, *ACS Nano*, 2014, **8**, 10640-10654.
30. B. Yang, F. Guo, Y. Yuan, Z. Xiao, Y. Lu, Q. Dong and J. Huang, *Adv. Mater.*, 2013, **25**, 572-577.

31. K.-W. Tsai, S.-N. Hsieh, T.-F. Guo, Y.-J. Hsu, A. K. Y. Jen and T.-C. Wen, *J. Mater. Chem. C*, 2013, **1**, 531.
32. S. J. Kerber, J. J. Bruckner, K. Wozniak, S. Seal, S. Hardcastle and T. L. Barr, *J. Vac. Sci. Technol., A*, 1996, **14**, 1314-1320.
33. J. S. Kim, P. K. H. Ho, D. S. Thomas, R. H. Friend, F. Cacialli, G. W. Bao and S. F. Y. Li, *Chem. Phys. Lett.*, 1999, **315**, 307-312.
34. F. Nüesch, L. J. Rothberg, E. W. Forsythe, Q. T. Le and Y. Gao, *Appl. Phys. Lett.*, 1999, **74**, 880-882.
35. Q. T. Le, E. W. Forsythe, F. Nüesch, L. J. Rothberg, L. Yan and Y. Gao, *Thin Solid Films*, 2000, **363**, 42-46.
36. X. Liu, C. Wang, L. Lyu, C. Wang, Z. Xiao, C. Bi, J. Huang and Y. Gao, *PCCP*, 2015, **17**, 896-902.
37. Z. Y. Zhong and Y. D. Jiang, *physica status solidi (a)*, 2006, **203**, 3882-3892.